Characteristics of Jet Impingement in a Side-Dump Combustor

Nagy S. Nosseir* and Shabtay Behar†
San Diego State University, San Diego, California

In a two-dimensional simulator of a side-dump ramjet combustor, flow visualization is used to investigate the impingement of two jets on each other. In this configuration, the two jets are introduced into the combustor through rectangular ports in its sides. The jets impinge upon one another at the plane of symmetry of the combustor, with an angle of impingement equal to 180 deg. Counter-rotating vortex pairs are generated in the impinging region. The axes of the vortices are parallel to the plane of symmetry of the combustor. Vorticity measurement indicates that the strength of these vortices changes periodically due to their stretching in the downstream direction of the combustor. The mechanism of vortex generation and the effects of the combustor's dimensions on it are investigated.

Nomenclature

d = side jet width, cm
D = dome length, cm
f = frequency of vortex generation, 1/sec
H = combustor width
ℓ = unit vector
L = length of the grid mesh = 1 cm
n = number of video movie frames over which ω_z is averaged
Re = Reynolds number = Ud/ν
t = time, s
S = displacement vector
V = velocity vector
x,y,z = coordinate system
ω_z = strength of axial vortices, 1/s
Ω_z = z component of local vorticity, 1/s, averaged over a mesh
λ = wavelength of velocity profiles modulation, cm
σ = standard deviation of λ

Subscripts
p = pulse
f = movie frame

I. Introduction

THE impingement of two jets on each other is an important feature of the flowfield of side-dump combustors. In these combustors, two or more jets are introduced through ports in its sides. Fluid mixing and the combustion process take place primarily in the impinging region of the jets. Therefore, an understanding of jet-to-jet impingement is important to achieving good combustion performance as well as arriving at possible solutions to combustion instabilities.

Surprisingly, fundamental research on jet-to-jet impingement is very limited despite the practical importance of the problem. Our initial approach was guided mainly by Powell's[1] mirror image concept. The concept indicates that the impinging of two jets separated by a distance H is theoretically equivalent to a single jet impinging on a flat plate placed at a distance $H/2$ downstream. The concept is plausible, although not proved yet, when applied in the impingement of laminar jets. However, the instabilities associated with the free jets before impingement cast serious doubts on the validity of the concept in a turbulent flowfield. These instabilities can be categorized as[2]: 1) "shear layer instability," which is associated with the initial thickness of the shear layer; and 2) "jet column instability," which is associated with the length of the potential core.[3] Crow and Champagne[4] showed that the jet reacts violently to external acoustic disturbances that have a frequency close to its column instability mode. A similar situation occurs in a side-dump combustor where the jets are exposed to strong pressure disturbances associated with the acoustic modes of the combustor.[5,6] The instabilities of the free jets of the combustor should strongly influence their impingement and the resulting flowfield is expected to be different from that of a jet-plate impingement.

The flowfield in a side-dump combustor can be viewed as a synthesis of a number of flow modules that include free turbulent jets, jet-to-jet impingement, and jet-wall impingement. Each module is capable of inducing flow oscillations that could trigger combustion instabilities. Clark[5,6] investigated combustion instabilities in two-inlet, side-dump ramjet combustors. His experiment focused on measuring low frequency pressure waves, in the range of 200–500 Hz, generated during the combustion process. (Pressure waves in this frequency range pose a serious problem in the development of liquid-fueled ramjet engines. These waves are believed to propagate upstream from the combustor and they interact with the inlet shock wave, causing inlet unstarting as well as degraded engine performance.[7]) Several tests were conducted in which the length of the inlet pipes and the combustor, flow rate, inlet total temperature, and equivalence ratio were changed. The dominant instability mode in all tests was at a frequency in the range from 250 to 320 Hz, with amplitudes of up to 20% of the total chamber pressure. Clark compared measured instability frequencies with the acoustic modes of the combustor. The acoustic modes were driven, in a no-flow situation, by a loudspeaker placed in the dome section of the combustor. In two of the cases tested, the dominant modes were associated with different longitudinal acoustic modes. The results indicate that 1) the approximately 300 Hz oscillation persisted regardless of the flow conditions or the combustor's dimensions, and 2) the combustor acoustics play a passive role; they augment pressure oscillations generated with frequencies close to the acoustic modes of the combustor. Clark speculated that the oscillations were triggered by the dynamics of the recirculatory flow at the dump location.

Flow visualization and measurement will be used here to study the dynamics of the flow inside a side-dump combustor.

Received Nov. 20, 1985; revision received Feb. 24, 1986.

*Associate Professor, Department of Aerospace Engineering. Member AIAA.
†Research Assistant, Department of Aerospace Engineering.

In particular, the present experiment will focus on the characteristics of the two jets, their behavior as they impinge on one another, and the effects of the combustor's dimensions on this behavior.

II. Experimental Facility

Figure 1 shows the two-dimensional combustor simulator that was built on a water table. In this closed-circuit system, the water was routed from the settling tank to the combustor through two channels . The channels had 90 deg bends and were equipped with turning vanes and screens to inhibit the generation of elbow vortices. The angle of impingement of the side jets on each other was 180 deg. The flow rate was controlled upstream of the settling tank with a Meriam Instrument Company flowmeter. The average Reynolds number based on the velocity and width of the side jets was $Re = Ud/\nu = 3000$. The coordinate system, with the y-z plane being the plane of symmetry of the combustor, is also shown in Fig. 1.

Two factors governed the design of the present facility to study the flowfield of the combustor: 1) flow visualization and observation are generally easier in low-speed (water) flows, and 2) effects of the cylindrical configuration of a real combustor are of secondary importance to the behavior of the flow. These two factors are not expected to interfere with understanding the fundamental behavior of the two impinging jets.

Visualization of the flow was conducted using two methods: Colored food dye was injected from hypodermic needles at different locations in the flowfield and hydrogen bubbles were generated from thin platinum wires by the electrolysis of the water. Flow measurements were combined with flow visualizations by the following means:

1) Frame-by-frame analysis of movies.

2) A laser beam was used to detect the oscillations of dye streak lines in the combustor. The laser was directed perpendicular to the water table surface from one side and was received from the other side by a photo cell (Fig. 2). The light intensity received by the cell changed every time the dye streak line intercepted the laser beam. One or two of these laser setups were used. The signals from the photo cells were fed to a two-channel spectral dynamics analyzer (model SD 375) that performed single and joint statistical analyses (e.g., correlation functions and spectra). In this method the streak line intercepted the laser beam two times in every cycle of streak line oscillation. Therefore, the frequency of measured signals was twice as much as the frequency of streak line oscillation.

3) A technique was developed to measure the strength of axial vortices, ω_z, in the impinging region of the combustor. A grid was made of fine platinum wires, 0.02 mm in diameter, and was supported in a plane perpendicular to the z axis of the combustor. The mesh size of the grid was 1 cm. The wires were electrically insulated, except for small parts at the mid-points between the wires' intersections (Fig. 3). Rectangular patches of hydrogen bubbles were generated from the uninsulated parts at intervals t_p. These were controlled by pulsing the grid with high voltage pulse-train (25 volts in amplitude). The velocity vector at each mid-point was calculated from the displacement of the bubbles using frame-by-frame analysis of video movies. The frame rate, $t_f = 1/30$ s, was approximately one order of magnitude smaller than t_p. This allowed us to vary the number of frames (n) over which the velocity vector was averaged with the fluctuation in the strength of vorticity. In this way, good sensitivity in measuring ω_z was maintained even when its value approached zero. The plane of the grid was illuminated by a thin sheet of light so that the hydrogen bubbles could be carried by the mean flow out of the camera's field of view before new bubbles were generated. This eliminated any confusion that might have occurred due to the presence of too many bubbles in the field of view.

Since our objective was to measure the fluctuation in the strength of a vortex rather than the vorticity at a point, the location of a vortex axis as a function of the time was first determined by previewing the movies. The strength of a vortex

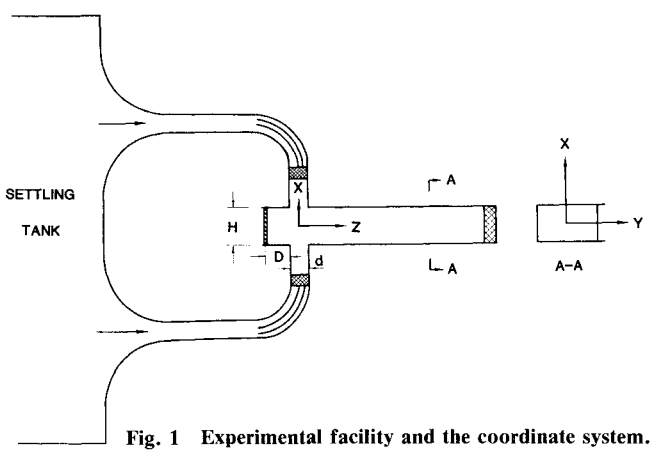

Fig. 1 Experimental facility and the coordinate system.

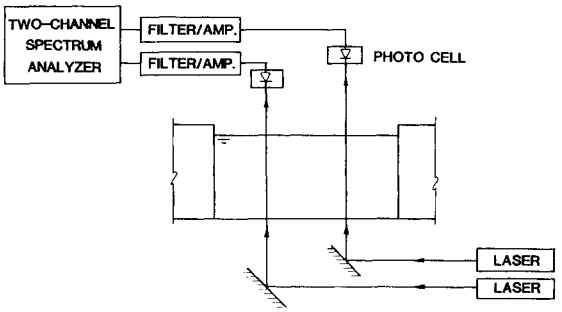

Fig. 2 Laser setup for measurement of frequency of oscillation of streak lines.

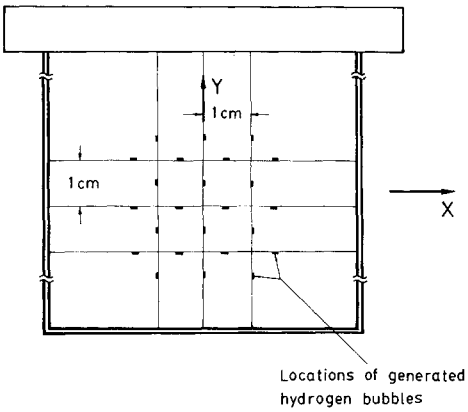

Fig. 3a Platinum wires grid for measuring ω_z.

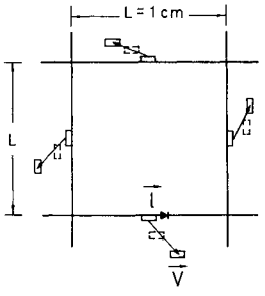

Fig. 3b Schematic of velocity vectors used in calculating the circulation around a grid mesh, averaged over two movie frames. The broken line rectangulars represent displaced bubbles after one frame.

was calculated by measuring the circulation around a grid mesh, whose centroid is nearest to the vortex axis, and dividing it by the area of the mesh (Fig. 3), using the following relation:

$$\omega_z(t) = \left[L \sum_{i=1}^{4} (V_i \cdot \ell_i)\right] \Big/ L^2 \qquad V_i = S_i/nt_f \qquad (1)$$

where V_i and S_i are the velocity and displacement vectors of the tracers generated at the mid-points of the sides of the square mesh, and ℓ_i is a unit vector along the sides of the mesh. The summation is carried over the indices, i, representing the sides of the mesh. Based on measurements (Table 1) discussed later, the length scale of generated vortices was of the same magnitude as λ_2, which is about three times larger than L. Therefore, we seldom encountered the presence of more than one vortex within a grid mesh.

The flow measurement and visualization were made approximately half-way between the free surface of the water and the table's surface so that effects of the free surface and the boundary layer were negligible.

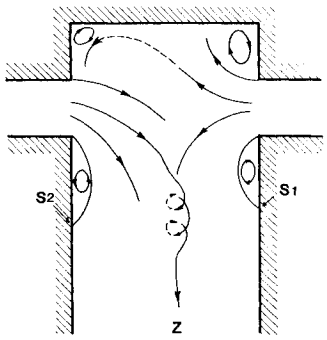

Fig. 4 Instantaneous streak lines pattern of the flowfield.

Fig. 5 Counter-rotating vortex pairs generated near the impinging plane.

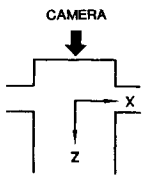

III. Experimental Results

General Characteristics of the Flowfield

The instantaneous streak line pattern of the flowfield is shown schematically in Fig. 4. The free jets impinged on each other and reattached to the side walls at points S_1 and S_2. Movies of the flow indicated that part of one jet (e.g., the right-hand jet) was deflected into the dome of the combustor at one moment, then a moment later it was deflected out while the other jet was deflected in. Oscillation of each jet into the dome was almost periodic and out of phase with the oscillation of the other jet. During these oscillations the impinging jets were never stable in a symmetrical pattern with respect to the plane of impingement (i.e., the mirror image concept was never achieved over a finite time period).

One of the most striking features of the flowfield was the generation of vortices in the impinging region of the two jets. The axes of these vortices were parallel to the z axis. The direction of rotation of the vortices varied in time between clockwise ($\omega_z < 0$) and counterclockwise ($\omega_z > 0$). The view from the dome side of a hydrogen bubble wire placed along the y axis (Fig. 5) indicated that each vortex was in fact a member of a chain of counter-rotating vortex pairs. This chain extended over the depth of the combustor. Therefore, at any instant of time, the total circulation around the z axis remained equal to zero. This was expected because of the geometric symmetry of the combustor with respect to the y-z plane, and the equal velocities of the two jets.

Since fluid mixing has a direct impact on the chemical reaction inside a combustor, we will discuss the important role these vortices play in the mixing process. Vorticity plays a two-fold role in mixing. Irrotational fluid is engulfed toward the vortex axis by the induced field of the mean vorticity. On the other hand, vorticity fluctuation, by stretching, for example, generates Reynolds stresses. Accordingly, fresh fluid that is entrained by the mean vorticity experiences fine-scale mixing brought about by vorticity fluctuation. This process was observed by Dimotakis and Brown[8] when mixing two chemically reacting fluids. The dynamics of the initial part of the shear layer was dominated by two-dimensional, large-scale vortices. The mixing process took

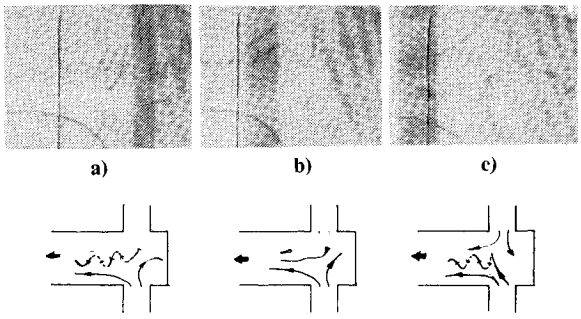

Fig. 6 Streak lines indicate a cycle of the fluctuation in the strength of a vortex generated in the impinging region of the side jets. a) $\omega_z < 0$, b) $\omega_z \simeq 0$, and c) $\omega_z > 0$. Note that the fluctuation in ω_z is associated with oscillation of a portion of either jet into the dome of the combustor, $Re = 3000$. (The broken and solid lines in the schematic drawing mark the lower- and upper-half of the vortex tube, respectively.)

Table 1 Wavelength of velocity profile modulation

U, cm/s	4	5	4	4	5
H/d	1.25	1.75	2	2.25	2.50
λ_1, cm	1.48	1.41	1.34	1.24	1.28
σ_1	0.14	0.07	0.08	0.1	0.06
λ_2, cm	3.20	3.05	2.87	2.30	2.62
σ_2	0.24	0.19	0.14	0.18	0.09
λ_2/λ_1	2.16	2.16	2.14	1.86	2.05

place in two stages. First, fluid from the mainstreams was engulfed by the large-scale vortices toward the center of the shear layer. Appreciable mixing between the two entrained fluids was not observed until the large-scale vortices broke down into fine-scale eddies. (The breakdown could have been due to the pairing between large-scale vortices.) This set the stage for a very rapid chemical reaction due to fine-scale mixing.

The Mechanism of Vortex Generation

The fluctuation in the strength of the generated vortices was found to be phase locked with the oscillation of the side jets into the dome. This is shown by a sequence of three frames taken from a video movie (Fig. 6). In this sequence, four streak lines were produced by injecting colored dye at two points in the exit plane of each jet. The upstream streak lines marked the portion of each jet that oscillated into the dome. In Fig. 6a, the upper jet is shown moving out of the dome; the vorticity is negative and its strength is augmented by stretching. In Fig. 6b, the upper jet is about to oscillate back; the vorticity is changing its sign here (i.e., $\omega_z = 0$). A cycle of oscillation is completed as the upper jet moves into the dome (Fig. 6c), when $\omega_z > 0$. In this process, the magnitude of ω_z reached two maxima during one cycle of jet oscillation. In other words, two vortices, one with a positive sign and one with a negative one, were generated during one cycle.

Measurements of ω_z were used to confirm these visual observations. The technique and equation used were discussed in Sec. II. The variation of vorticity with time is shown in Figs. 7 and 8. The time intervals (nt_f) used in averaging the vorticity are much smaller in Fig. 7 than in Fig. 8. In addition, there is a fundamental difference between the two figures which displays the flexibility of the measuring technique. Figure 7 shows an estimate of vorticity around the centroid of a grid mesh, i.e., the fluctuation of *local* vorticity, Ω_z. Because the generated vortices are not fixed in space, Ω_z measurement captures approximately a half cycle of the fluctuation in the strength of a vortex. The negative sign vortex captured in the figure has a period of 3.2 s. However, in Fig. 8, the temporal location of the generated vortex axis was predetermined before ω_z was measured. The fluctuation in ω_z confirms the visual observations; the average period of the fluctuation is approximately the same as in Fig. 7. As is expected from the geometric similarity of the two jets with respect to the impinging plane, the average value of ω_z is approximately equal to zero.

Vortex generation can be explained by analyzing the velocity profiles of the two jets. The timelines of Fig. 9 represent velocity profiles in a plane parallel to the x-y plane ($z = -d/4$). The lines are straight near the jet exit planes, indicating uniform velocity profiles. As the two jets approach the impinging plane, modulation of the velocity profiles occurs. The velocity modulation of one jet is out of phase with the modulation of the other. This is due to the continuity principle. At any plane parallel to the x-z plane, the deflection of one jet into the dome would cause a decrease in its velocity. Simultaneously, the corresponding velocity of the other jet would increase as it accelerates in the downstream direction. In an adjacent plane, the opposite would occur, resulting in the observed out-of-phase modulations. Vortex pairs are generated due to the out-of-phase modulation in the velocity profiles of the impinging jets (as is shown in Fig. 9). The

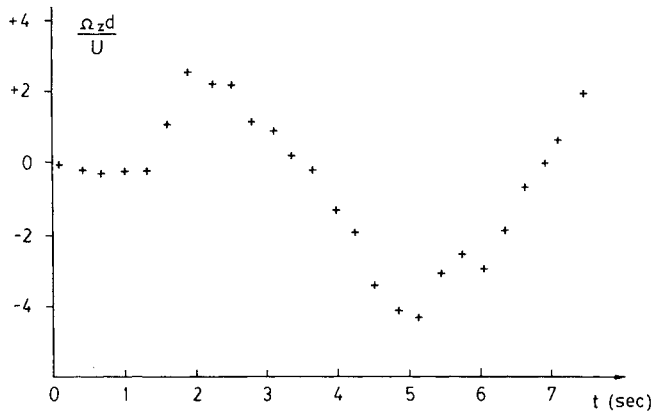

Fig. 7 Fluctuation of vorticity at a point with coordinates (0, −0.85, 2) in cm, and $U = 4.5$ cm/s.

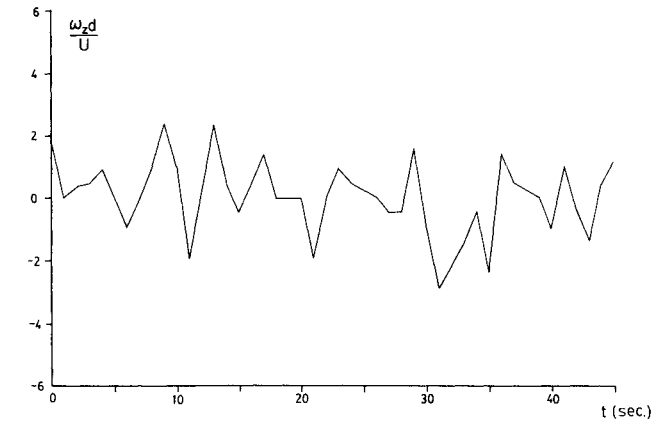

Fig. 8 Fluctuation of the strength of a generated vortex.

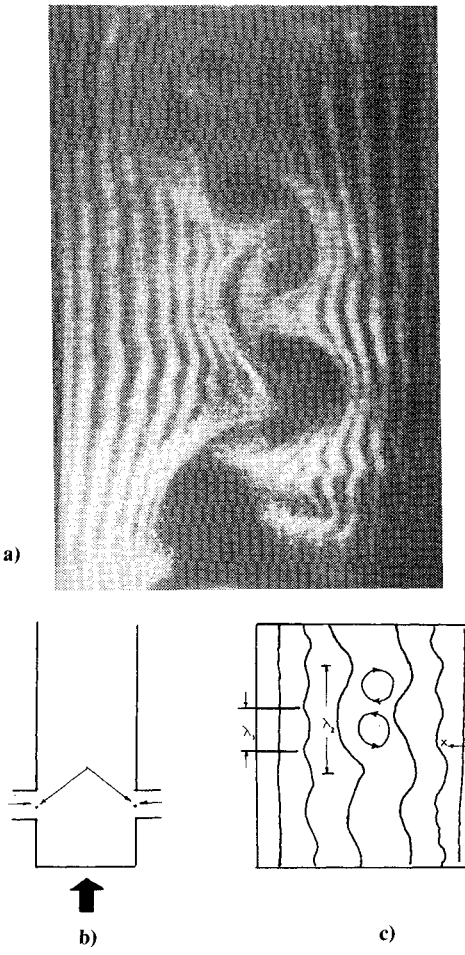

Fig. 9 a) Modulation of the velocity profiles of the impinging jets as shown by the time lines. b) A camera view from the dome section of time lines generated at the exit planes of the jets. c) A schematic drawing of the generated vortex pair and its location relative to the modulation of the velocity profiles.

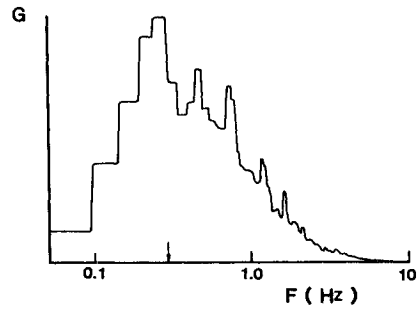

Fig. 10 Spectrum of vortex generation, measured from the oscillation of the jets into the dome of the combustion; $H=9$ cm, $D=d=4$ cm, and $U=4$ cm/s.

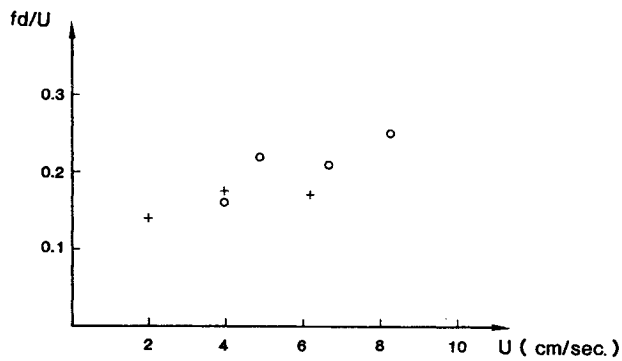

Fig. 11 Variation of the Strouhal number (fd/U) with velocity. Data are based on o laser measurement; + analysis of video movies; $H=8$ cm, $D=d=4$ cm, and $U=4$ cm/s.

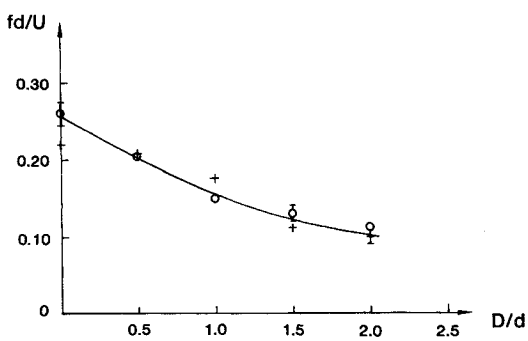

Fig. 12 Variation of the Strouhal number with the dimensionless dome length (D/d).

following measurement suggests that the wavelength of the velocity profile modulation is associated with an instability of the free jets along their major axes.

Effects of the Combustor Dimensions on Vortex Generation

The wavelength (λ) of the velocity modulation of the jets and its standard deviation (σ) are presented in Table 1. Two wavelengths were observed (Fig. 9). The first wavelength, λ_1, represents the velocity modulation developed upstream of the impinging region. Yokobori et al.[9] studied the impingement of a two-dimensional jet on a flat plate. They also observed modulations of the impinging shear layers of the jet. The average wavelength of the modulation was equal to 1.1 cm for a nozzle-to-plate distance of 6 nozzle widths. This value is within the range of λ_1 in the table. Furthermore, the velocity fluctuation profiles along the major axis of a free eliptical jet[10] exhibited similar modulations with a wavelength equal to approximately 1 cm. The second wavelength, λ_2, is approximately equal to the size of a vortex-pair, and, according to visualization, is associated with the vortex generation. The ratio λ_2/λ_1 is equal to 2, approximately, which suggests that λ_2 is a subharmonic of λ_1.

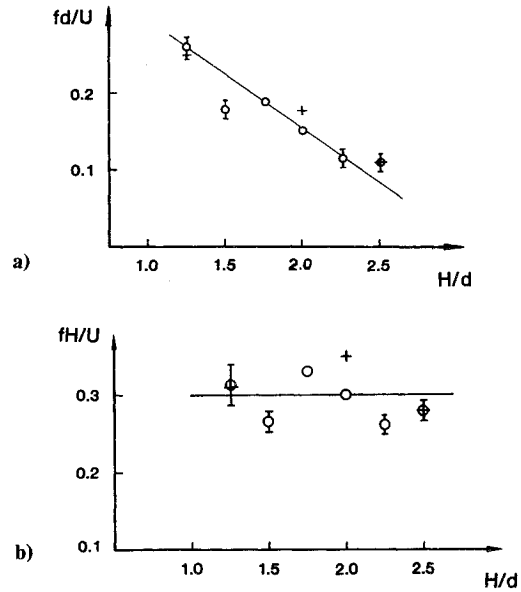

Fig. 13 Variation of the nondimensional frequency of vortex generation with the combustor width, a) fd/U vs H/d and b) fd/U vs H/d: $U=4-7$ cm/s and $D=d=4$ cm.

Effects of the combustor dimensions and flow velocity on the frequency of vortex generation were examined by measuring the frequency of jet oscillation into the dome. An example of the spectra measured by the laser method is shown in Fig. 10. According to this method, the frequency f of the fundamental spectral peak is twice the frequency of jet oscillation, as is the frequency of vortex generation. Therefore, f represents the frequency of vortex generation. The fundamental peak of the spectrum (Fig. 10) corresponds to a period approximately equal to those measured in Figs. 7 and 8.

The frequency f increases slightly when the velocity U is increased (Fig. 11). It has an average dimensionless value of $fd/U=0.2$. This value is in the range of dimensionless combustion instability frequencies measured by Clark.[5,6] However, f decreases when the dome length D is increased (Fig. 12). The trend in Fig. 12 can be qualitatively explained using the mirror image concept. The impinging jet would correspond to a combustor with D equal to infinity. The frequency in this case would be equal to zero. Therefore, as shown in the figure, f would asymptotically approach zero as D is increased.

Finally, Fig. 13a indicates that f decreases with the combustor width H. However, the frequency normalized with respect to H and U (Fig. 13b) is unchanged with increasing H/d, which indicates that H is the characteristic length for jet oscillation and, accordingly, plays an important role in vortex generation.

IV. Conclusion

The behavior of two jets impinging on each other in a side-dump combustor was investigated. The impingement generated vortices with axes along the downstream direction and parallel to the plane of impingement. The strength and direction of rotation of the vortices were phase locked with the oscillations of the jets in and out of the dome of the combustor. In chemically reacting jets, this phenomenon would produce periodic releases of high energy levels because of the enhanced mixing associated with these vortices.

Acknowledgment

The support of the Office of Naval Research under Contract N0014-84-K-0373 is gratefully acknowledged.

References

[1]Powell, A., "Aerodynamic Noise and the Plane Boundary," *Journal of the Acoustical Society of America,* Vol. 32, 1960, pp. 982-990.

[2]Ho, C.M. and Huerre, P., "Perturbed Free Shear Layers," *Annual Review of Fluid Mechanics,* Vol. 16, 1984, pp. 365-424.

[3]Kibens, V., "Discrete Noise Spectrum Generated by an Acoustically Excited Jet," *AIAA Journal,* Vol. 18, 1980, pp. 434-441.

[4]Crow, S.C. and Champagne, F.H., "Orderly Structure in Jet Turbulence," *Journal of Fluid Mechanics,* Vol. 48, 1971, pp. 547-591.

[5]Clark, W.H., "Experimental Investigation of Pressure Oscillations in a Side Dump Ramjet Combustor," *Journal of Spacecraft and Rockets,* Vol. 19, Jan./Feb., 1982, pp. 47-53.

[6]Clark, W.H., "Geometric Scale Effects on Combustion Instabilities in a Side Dump Liquid Fuel Ramjet," 19th JANNAF Combustion Meeting, CPIA Vol. 1, No. 366, pp. 595-604.

[7]Waugh, R.C. et al., "A Literature Survey of Ramjet Combustor Instability," *Proceedings of the ONR/AFOSR Workshop,* Atlanta, GA, CPIA No. 375, pp. 1-13.

[8]Dimotakis, P.E. and Brown, G.L., "The Mixing Layer at High Reynolds Number: Large-Structure Dynamics and Entrainment," *Journal of Fluid Mechanics,* Vol. 78, Pt. 3, 1976 pp. 535-560.

[9]Yokobori, S., Kasagi, N., and Hirata, M., "Characteristic Behavior of Turbulence in the Stagnation Region of a Two-Dimensional Submerged Jet Impinging Normally on a Flat Plate," *Proceedings of 1st International Symposium on Turbulent Shear Flows,* University Park, PA, April 1977, pp. 3.17-3.25.

[10]Gutmark, E., Schadow, K.C., Parr, D.M., Harris, C.K., and Wilson, K., "Mean and Turbulent Structures of Noncircular Jets," AIAA Paper 85-0543, Jan. 1985.